Solid-State Electronics 52 (2008) 1407–1413

Contents lists available at ScienceDirect

Solid-State Electronics

journal homepage: www.elsevier.com/locate/sse

Degradation of CMOS image sensors in deep-submicron technology due to γ-irradiation

Padmakumar R. Rao [a,*], Xinyang Wang [a], Albert J.P. Theuwissen [a,b]

[a] Electronic Instrumentation Lab, Delft University of Technology, Delft, The Netherlands
[b] Harvest Imaging, Belgium

ARTICLE INFO

Article history:
Available online 13 May 2008

The review of this paper was arranged by Jurriaan Schmitz

Keywords:
CMOS image sensors
Gated-diodes
Radiation hardness
STI
Spectral response

ABSTRACT

In this work, radiation induced damage mechanisms in deep submicron technology is resolved using finger gated-diodes (FGDs) as a radiation sensitive tool. It is found that these structures are simple yet efficient structures to resolve radiation induced damage in advanced CMOS processes. The degradation of the CMOS image sensors in deep-submicron technology due to γ-ray irradiation is studied by developing a model for the spectral response of the sensor and also by the dark-signal degradation as a function of STI (shallow-trench isolation) parameters. It is found that threshold shifts in the gate-oxide/silicon interface as well as minority carrier life-time variations in the silicon bulk are minimal. The top-layer material properties and the photodiode Si–SiO_2 interface quality are degraded due to γ-ray irradiation. Results further suggest that p-well passivated structures are inevitable for radiation-hard designs. It was found that high electrical fields in submicron technologies pose a threat to high quality imaging in harsh environments.

1. Introduction

CMOS active pixel sensors (APS) rival CCDs in domains that include low power operation, on-chip integration of analog and digital circuitry as well as cost effectiveness. Since these sensors are utilized for applications involving the detection of signals as low as a few electrons as well as high energy photons (especially for medical/outer-space applications), radiation tolerance of such devices is of primary concern. All possible radiation effects are usually grouped into three basic types: transient effects (not included in this work), ionization damage and displacement damages [1–3]. Ionization damage is the dominant mechanism when energetic photons (γ and X-rays) interact with solid-state matter. For main stream silicon CMOS, the major concerns due to ionization damage are charge build-up in the gate dielectric, radiation induced interface levels, and the displacement of lattice atoms in the bulk. The introduction of discrete energy levels at the Si-SiO_2 interface leads to increased generation rates and thus higher surface leakage currents. Similarly, displacement of lattice atoms in the bulk leads to modified minority carrier life-times and increased bulk-generated leakage currents [2–6]. In this work, we have utilized a simple structure called as a gated-diode (GD) for resolving these mechanisms. An overview of its operation as well as experimental results is provided in Section 2. Section 3 deals with the γ-ray irradiation effects on 4-T (4 transistor) CMOS image sensors. These sensors are currently state-of-the-art in the image sensor world. They utilize a p^+ pinning layer that shields the photodiode from surface effects that contribute to the leakage mechanism. The doping of the photodiode layers are chosen such that the photodiode is completely depleted. A model for the spectral response of such a sensor is derived in Section 3.1 and irradiation effects are studied utilizing the model. One of the most dominant dark current mechanisms in these structures are the defective sidewalls and the edges of shallow trench isolations (STIs) separating the photodiodes [7,8]. The emission rate from the defects is also enhanced by local electrical fields via the Poole–Frenkel effect as well as the phonon-assisted tunneling [5,9]. This in turn increases the shot noise and fixed-pattern noise (FPN) of the image sensor [7]. The impact of irradiation on these effects is studied in Section 3.2. Finally, conclusions are drawn in Section 4.

The γ-ray (1.17–1.33 MeV) dose used for the experiments was from 0 to 1000 Gray in steps of 200 Gray, with a dose rate of 75.9 Gray/min. All the test structures for the experiments were fabricated in Philips' 0.18-μm CMOS technology.

2. Gated-diodes

2.1. Gated-diode (GD) theory

The GD (Fig. 1) is a structure obtained by placing a diffusion region (drain) contiguous to a gate region. The application of a

* Corresponding author.
E-mail address: p.rao@ewi.tudelft.nl (P.R. Rao).

0038-1101/$ - see front matter © 2008 Elsevier Ltd. All rights reserved.
doi:10.1016/j.sse.2008.04.023

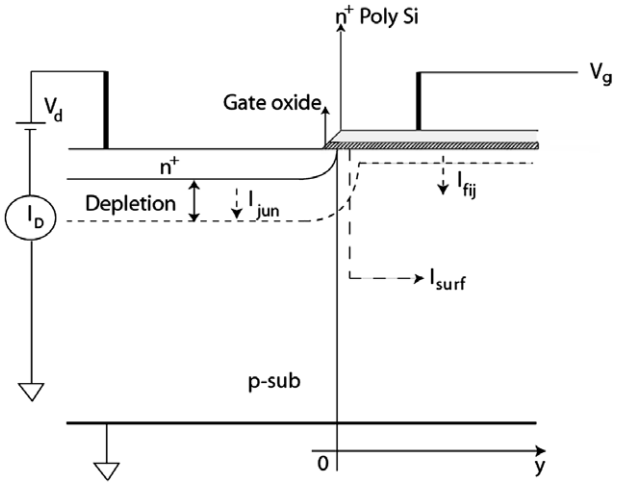

Fig. 1. The gated-diode structure and leakage components.

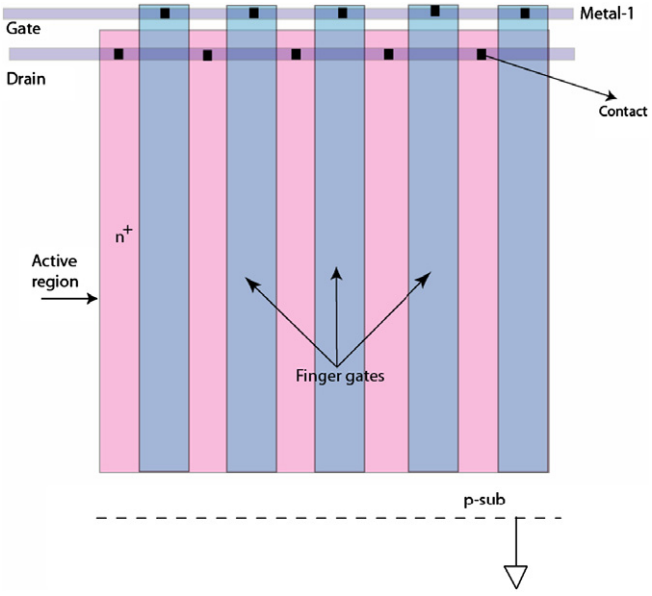

Fig. 2. Finger gated-diode structure; gate (diode) length = 1 μm, FGD length = 300 μm, FGD width = 300 μm, number of gates (diodes) = 150.

reverse bias V_d on the drain lowers the quasi-fermi level for electrons, thus modulating the gate voltage V_g required to induce an inversion. In this non-equilibrium case and under the simplifying assumption that potential variation in a direction parallel (y-axis) to the surface is negligible, sweeping the voltage of the overlapping gate V_g through the regimes of accumulation, depletion and strong inversion while monitoring the reverse current I_D, helps resolve the surface leakage component I_{surf} as well as the bulk (field-induced) leakage component I_{fij}. These leakage components help establish two important device parameters, s_0 the surface recombination velocity (SRV) at the gate-oxide/silicon interface and τ_0, the generation life-time of minority carriers in the silicon bulk using the fundamental GD equations [13]. They are temperature-dependent parameters, whose temperature dependence is determined by the energy position of the dominant generation center and of the center capture cross sections [10]. The current I_{fij} is due to the generation via the G–R (generation–recombination) centers in the depletion region of the field-induced junction close to the surface under the gate and hence provides information about the carrier life-times in this region of interest [11,12]. The recombination at the surface is usually described by considering it as a plane sink, with a gradient of carrier concentration close to it. The surface analogue of a minority carrier life-time in the bulk, s_0 provides a conveniently homogeneous boundary condition for the excess minority carrier concentration.

s_0 (as well as $1/\tau_0$) can be related to the interface trap density N_{it} in the interface (bulk) by the equation, s_0 (or $1/\tau_0$) = $\sigma v_{th} N_{it}$ where σ is the carrier capture cross-section area in the interface (bulk), and v_{th} is the thermal velocity (10^7 cm/s) [13].

2.2. Finger gated-diode (FGD) experimental

Fig. 2 shows the schematic of the fabricated GD. The finger-gates were designed to preserve the required gate (diode) area to gate (diode) length and extract the necessary parameters. Fig. 3a shows the I–V characteristics of a FGD. The fast-centers at the Si–SiO_2 interface are responsible for the increase in the leakage current until threshold. The values of s_0 and τ_0 for a virgin FGD device from the I–V curves were calculated to be 2.8 cm/s and 3.5 μs, respectively. Fig. 3b shows the response of the FGD to an irradiation dose of 200 Gray. An obvious increase in the response can be seen after irradiation. The mechanism for this shift is an increase in the number of interface traps in the surface and/or in the bulk that leads to a higher leakage current. The point of inversion of the curves remained unchanged indicating that no charge

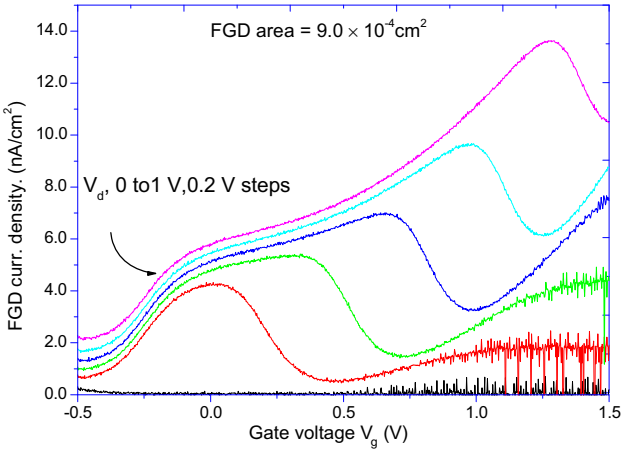

Fig. 3a. FGD I–V curves.

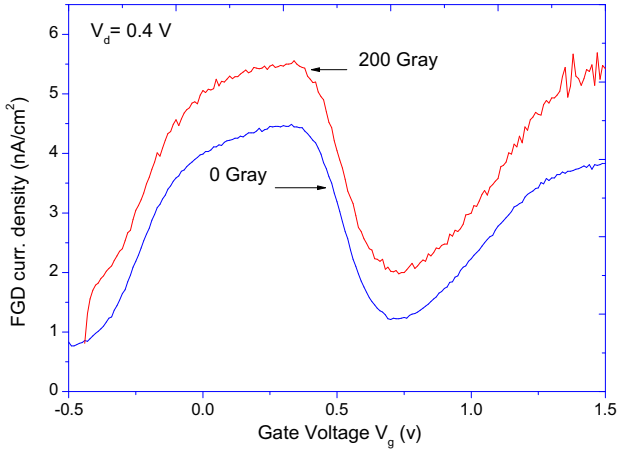

Fig. 3b. Radiation response of the FGD to a irradiation dose of 200 Gray.

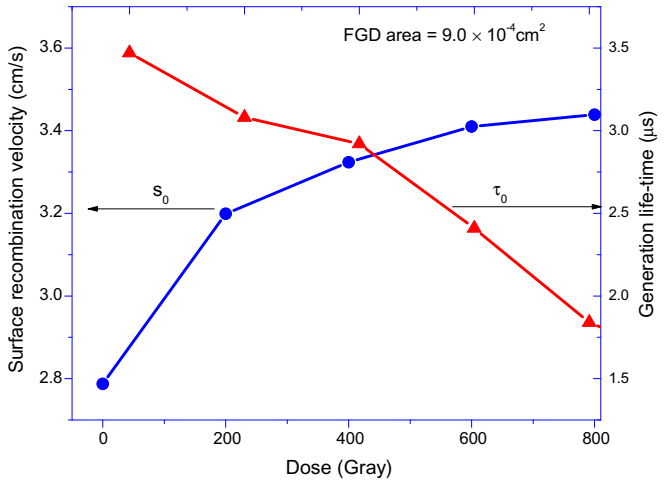

Fig. 4a. s_0 and τ_0 resolved using the FGD.

trapping has occurred in the SiO_2 region that can shift the flat-band or threshold voltages. Fig. 4a shows the variation of s_0 and τ_0 as a function of radiation dose resolved using the FGD. The surface component increases monotonically and saturates at higher doses. The bulk component, on the other hand, exhibits a rapid change after 400 Grays. The leakage currents reverse-computed from the s_0 and τ_0 parameters are shown in Fig. 4b. The knee-point for the bulk component of the leakage current in the figures can be explained by the fact that radiation-induced defects are divacancy and oxygen-vacancy (O-V) centers which are amphoteric [3]. Radiation-induced electron traps saturate at high radiation doses, increasing the density of excess electrons reaching n^+ drain region. An increase in the radiation induced leakage current density with a slope in the range of a few pA/cm^2/Gray is observed for both the surface as well as the bulk component.

Ionizing radiations generate holes that increase the oxide positive charge. The dispersive transport phenomenon in the SiO_2 can be modeled using the concept of small polaron hopping, called as CTRW (continuous-time random walk). The characteristic time scale of the hole transport process in the oxide (t_s), at a temperature (T), for the electric field in the oxide (E_{ox}) and the oxide thickness (t_{ox}) is given by [22],

$$t_s = t_{s0}\left(\frac{t_{ox}}{a}\right)^{\frac{1}{\alpha}} e^{\left(\frac{\delta_0 - 0.5qaE_{ox}}{kT}\right)} \quad (1)$$

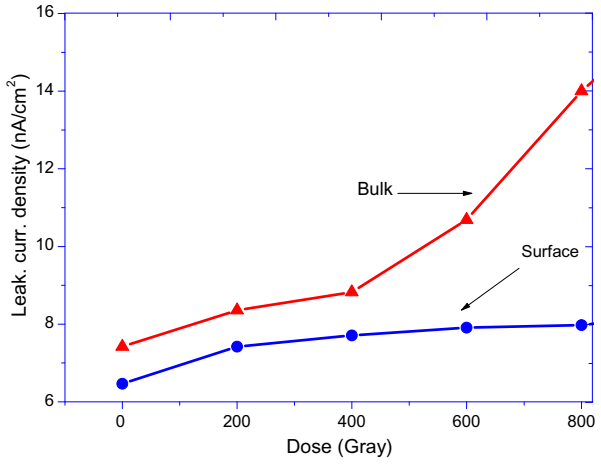

Fig. 4b. The reverse-computed current components using the obtained s_0 and τ_0 values.

where a is the average hopping distance in the direction of the electric field, δ_0 and t_s^0 are constants and $\alpha = 0.25$ for SiO_2. The transport process varies with the fourth power of the oxide thickness rendering modern deep submicron process ($t_{ox} \approx 4$ nm) radiation hard [21]. This also means that threshold shifts are negligible for this process as was confirmed by observing the inversion point of the I–V curves of the FGDs before and after irradiation. This is especially encouraging since 4-T CMOS image sensors include in-pixel amplifiers and transistors for its operation. Radiation induced threshold as well as gain variation in these transistors will be minimal.

Further, since the epi-layer thickness of modern CMOS technology is only a few micrometers, degradation of spectral response of such sensors due to carriers collected through diffusion (which is a function of minority carrier life-time) would be negligible. It should however be noted that for specialized sensors which rely more on the collection of diffused carriers (and hence thicker substrates) irradiation damage especially to the longer wavelength region will be more pronounced.

The spectral response degradation also manifests through changes in top-layer materials that form as part of the fabrication process above the photodiode element as well as its Si–SiO_2 interface. Such effects will be dealt in the following section.

3. CMOS image sensors

3.1. Spectral response: Model and experiment

A 4-T APS structure, shown in Fig. 5a, is a popular and rapidly improving solution to high quality image sensing. The p^+ pinning layer is used on top of the photodiode to shield it from surface effects and hence minimize surface leakage currents. The charges that are collected in the photodiode are transferred to the floating diffusion node (FD) via the transfer gate (TX), and subsequently read-out through a source follower (SF). This pixel area is considered to be the most vulnerable to the effects of radiation.

An analytic model for the internal spectral response of such a pinned photodiode can be derived by solving the continuity equation of a usual p^+/n photodiode (Fig. 5b) by using an equivalent diode reverse voltage V_{dp}, which represents the depleted diode. The contribution from the p-type epitaxial region is included for the contribution from carriers collected through diffusion. Since the penetration of the depletion region into the highly doped pinning region is negligible, this solution is a very good approximation to the spectral response of the pinned photodiode. The p^+ region is considered to have a Gaussian profile for the solution. The diffusion

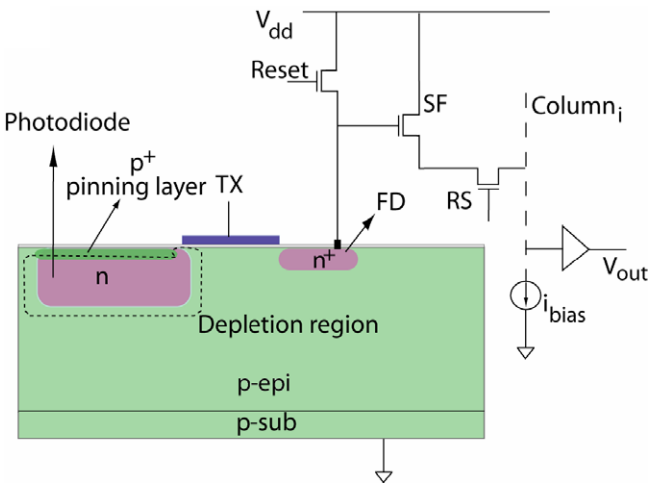

Fig. 5a. A 4-T APS structure.

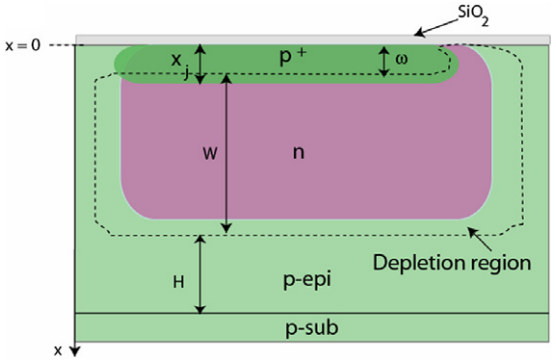

Fig. 5b. The schematic and relevant parameters of the p⁺/n/p-epi photodiode needed for deriving the analytic spectral response model.

length L_A may be considered to be small compared to the minority carrier (electrons) diffusion length $L_n = \sqrt{(D_n\tau_n)}$ where D_n is the diffusion coefficient and τ_n is the carrier life time, resulting in a simplified continuity equation,

$$\frac{\partial^2\Delta n}{\partial r^2} - r\frac{\partial\Delta n}{\partial r} - \Delta n = -\frac{F_0\alpha}{D_n}2L_A^2 e^{-\alpha\sqrt{2}L_A r} \quad (2)$$

where Δn is the excess minority carrier electrons in the p⁺ region, F_0 is the photon flux incident on the front surface whose reflection coefficient is zero, α is the absorption coefficient and r is $\frac{x_n}{\sqrt{2}L_A}$, where x_n is the depletion width in to the p⁺ region. The minority carriers lost in the front surface interface ($x = 0$) is governed by the relationship

$$s\Delta n|_{x=0} = D_n\frac{\partial\Delta n}{\partial x}|_{x=0} + \mu_n E\Delta n|_{x=0} \quad (3)$$

where s is the front surface recombination velocity. The concentration of excess carriers at the boundary of the depletion region ($x = \omega$) with a reverse bias V_{dp}, can be determined by the diode equation

$$\Delta n|_{x=\omega} = \frac{n_i^2}{N_A}\left(e^{\frac{qV_{dp}}{kT}} - 1\right) \quad (4)$$

where n_i is the intrinsic carrier concentration and N_A is the acceptor concentration. An analytic solution based on a power series can be a used to solve (2)–(4) [14]. Recombination in the space charge region is not considered. The contribution from the epitaxial region can be given as [15],

$$\frac{qF_0\alpha L_n}{(\alpha^2L_n^2 - 1)}e^{-\alpha(x_j+W)} \times \left(\alpha L_n - \frac{\cosh\left(\frac{H}{L_n}\right) - e^{(-\alpha H)}}{\sinh\left(\frac{H}{L_n}\right)}\right) \quad (5)$$

with the assumption of an infinite recombination rate at the epitaxial/substrate interface. Here x_j is the metallurgical junction depth of the p⁺/n diode, W is the depletion width and H is the thickness of the neutral p-region.

We attempt to resolve the radiation induced degradation mechanisms by fitting the response curve with the variables s (the surface recombination velocity) that affects the photons in the shorter wavelengths, and an attenuation factor ξ_i that was noticed on the irradiated devices. The image sensors used for the experiments have the properties listed in Table 1. Standard CMOS process parameters have been used for simulation purposes.

The variation of the spectral response as a function of s obtained through the developed model is shown in Fig. 6. The value of s is seen to significantly affect the response of the sensor towards shorter wavelengths, since electrons are generated very close to the interface for these photons.

Table 1
Sensor characteristics

Parameter	Value
Pixel pitch	3.5 μm
Conversion gain (g)(photon shot-noise method)	40 μV/e⁻
Transfer gate length	0.6 μm
Operating voltage	3.3 V
Integration time	6.4 ms

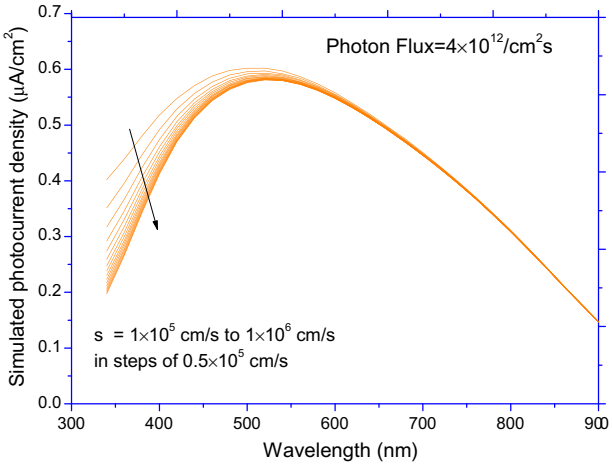

Fig. 6. Simulation of the variation of spectral response with varying surface recombination velocity (s).

Fig. 7 shows the normalized spectral response (sensors output in digital number (DN) compensated for dark signal/input optical power determined through a calibrated photodiode) of radiated as well as un-irradiated devices. The equivalent reverse voltage V_{dp} for the model was found to be 1.2 V resulting in a total depletion width of ~1.6 μm. The apparent p-region epi-depth was obtained at 10 μm. The deviation of this value from the physical epi-layer thickness of ~4 μm can be explained by the contribution of photo-generated electrons from the substrate which was neglected in the model. A very good fit for all the curves is obtained by using an attenuation factor ξ_i as well as the term for surface recombination velocity, $s = s_{eff}$.

From Section 2.2, it can be seen that there is negligible change in the threshold as well as gain of in-pixel transistors due to irradiation. Thus the parameter ξ_i can be decoupled from such electri-

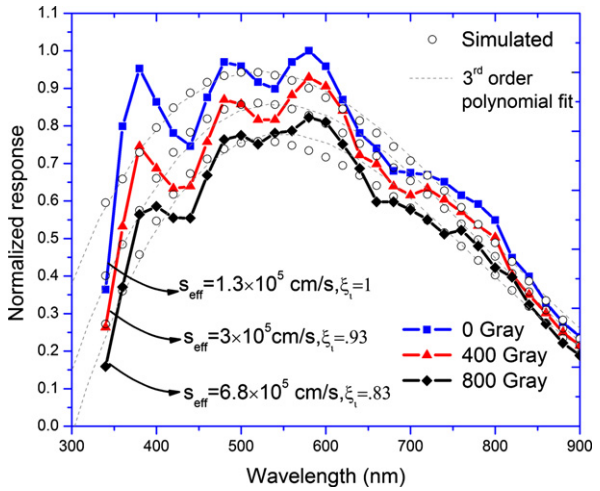

Fig. 7. Spectral response of radiated and un-irradiated sensors and the fit.

cal variations and related mainly to optical changes in the top-layer material stack of the photodiode. Also, it is worthwhile to note that only an effective value for s can be determined by this approach since wavelength-depended properties of the optical stack has not been included in the model. Nevertheless, the relative change in this parameter offers insight into the degradation of the Si–SiO_2 interface quality of the photodiode element.

The extracted parameters indicated in Fig. 7 reveal monotonic optical stack degradation as well as a change in the Si–SiO_2 interface effects. High energy rays such as γ-rays change the material properties of the materials they penetrate and mainly interact through electronic excitation, electronic ionization and atomic displacements. As a result, color centers can be introduced in the material [16], although this mechanism can be considered to be small for the dose range considered in this study. A combination of this effect along with a change in the reflection and/or multi-layer interference effects could better explain the attenuation observed. From Fig. 7, a smoothening of the sharp peaks found in the un-irradiated devices can be seen on radiated devices which can also be explained by this hypothesis. Clearly, further studies are needed to establish the mechanisms by which the optical degradation occurs. We are currently studying the effects of radiation on some commonly used materials that form on top of the photodiode in advanced CMOS processes for better understanding this phenomenon.

The variation of the lifetime in the epi-layer does not have much effect in the present sensor, with a thickness of a few micrometers. Since γ-ray irradiation do not produce significant displacement damages, the change in τ_n as a function of radiation dose can be safely neglected.

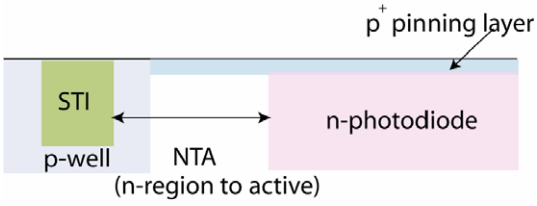

Fig. 8. Layout schematic of the pixels.

3.2. Dark signal degradation

For sub-0.25 μm processes, STI is the only viable scheme of achieving high packing densities [17]. The STI is considered to be the prominent mechanism of leakage current in pinned photodiodes [7,19]. The generation rate can be characterized through the

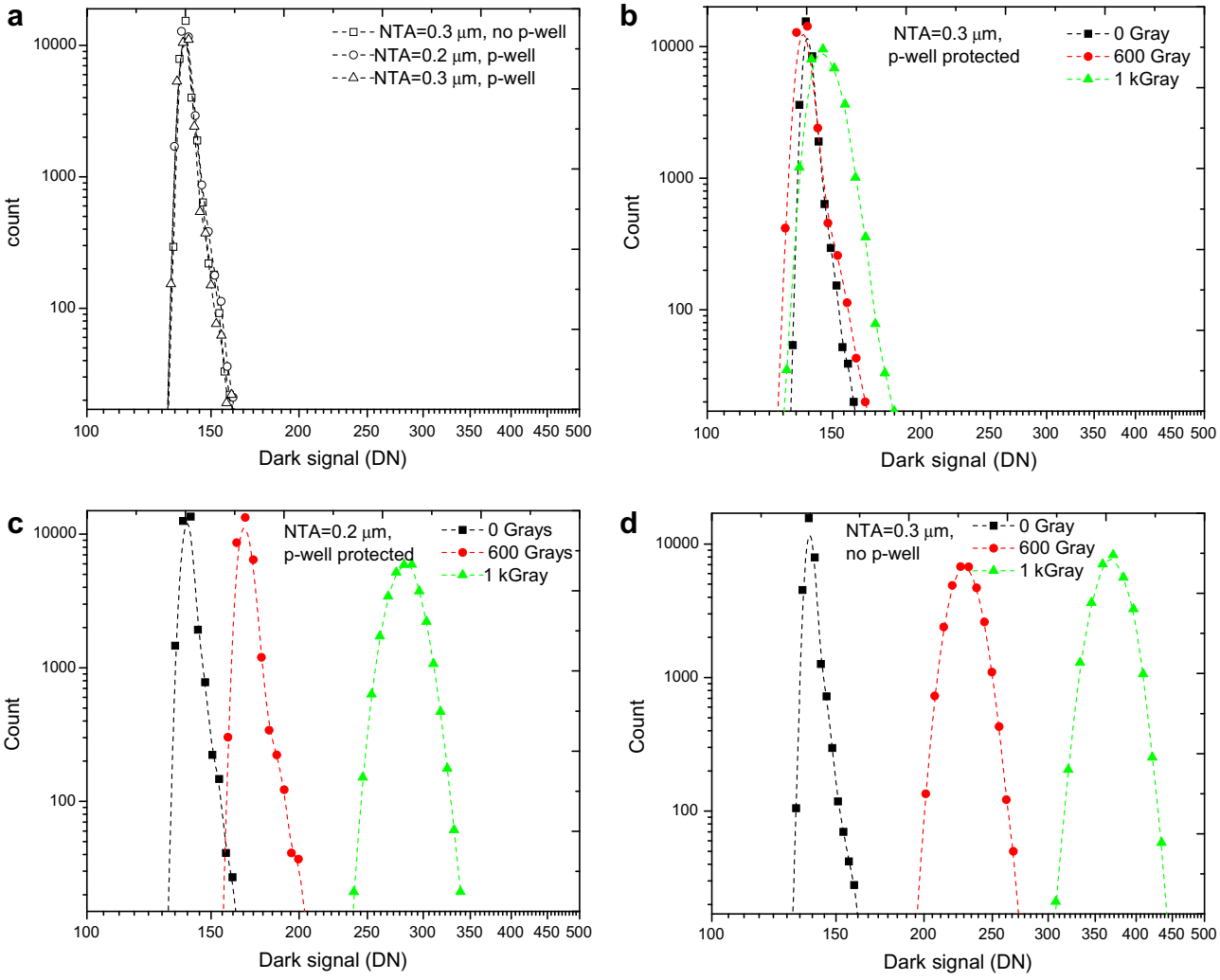

Fig. 9. (a) Histogram of the dark signal for the un-irradiated sensors, (b) histogram of the dark signal for sensor with NTA = 0.3 μm, p-well protected, (c) histogram of the dark signal for sensor with NTA=0.2 μm, p-well protected, (d) histogram of the dark signal for sensor with NTA = 0.3 μm, no p-well protection.

surface recombination/generation velocity at the interface and also by the generation lifetime in the bulk of the STI, the interface effects being prominent [8]. Protecting the STIs by p-well structures has proved useful against STI induced leakage mechanisms. But not much work has been done to characterize the effect of such structures in radiative environments especially on image sensors. Test structures (Fig. 8) with and without p-well protection were fabricated for two different "p-well to active region" distances (NTA) to estimate the degradation due to these configurations.

The histograms of the dark signal of the sensors (Fig. 9a–d) reveal that the radiation-induced degradation mechanism is sensitive to the nature and the location of the STI. The largest degradation is seen in structures that have unprotected STIs. Further, structures that have the STI closer (NTA = 0.2 μm) to the photodiode is seen to degrade faster than the structures that have the STI further apart (NTA = 0.3 μm). A larger value of NTA results in higher immunity to radiation damage, but this value should be optimized so the sensitivity and saturation level of the sensor is not overly sacrificed. Since the doping density of the p-well region is relatively higher than that of n-type region of the photodiode, the STI is isolated from the depletion region during integration for structures with p-well protection [19]. This explains the lower dark current from these structures, and the also the slower degradation of these structures to irradiation.

The Arrhenius plot of the mean dark current of un-irradiated as well as radiated sensors is shown in Fig. 10. The activation energy of silicon devices such as CMOS image sensors usually lie anywhere between E_g (1.2 eV; characteristic of a diffusion process) and $E_g/2$ (0.56 eV; characteristic of a thermal generation process). Generally, at room temperature, the thermal generation process dominates the diffusion mechanism. However, pixels with a low dark current may also see a diffusion current dependence. Upon irradiation of the sensors, it was found that the average activation energy of the sensors was reduced. Processes like trap-assisted tunneling and field-enhanced emissions have been speculated to play a role in this behavior. The emission rate from a defect that is located in a high local electric field is believed to increase dramatically [6]. To further investigate this phenomenon, the activation energies of some 1000 pixels as a function of dark current (Fig. 11) was extracted. The activation energy of the pixels forms a band from 1.2 eV to 0.56 eV, with most of the pixels being concentrated around the mean activation energy of the sensor. Pixels with lower activation energies were seen to exhibit a higher dark current. These findings reveal a field-enhancement mechanism in

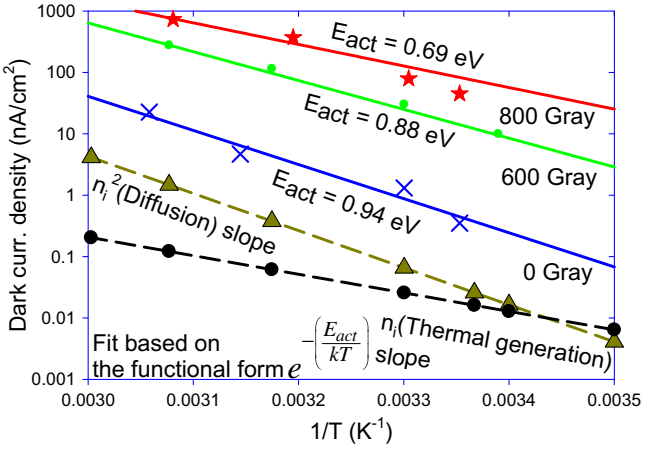

Fig. 10. Arrhenius plot of the dark current of sensor (NTA = 0.3 μm, no p-well). The scaled representative slopes for n_i (intrinsic carrier concentration) and n_i^2 have been plotted for comparison.

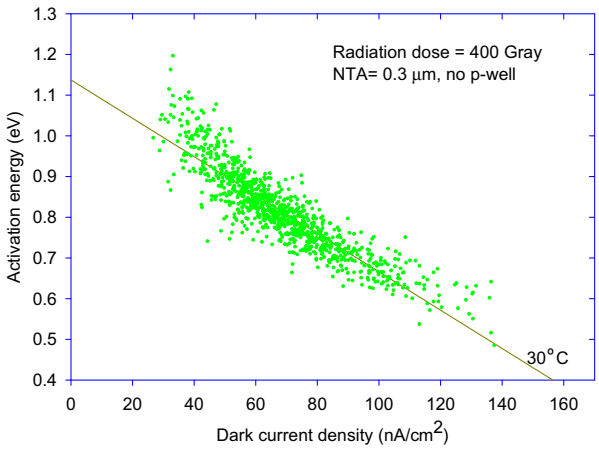

Fig. 11. Leakage current vs. activation energy of 1000 pixels (NTA = 0.3 μm, no p-well).

action [1,6]. The Poole–Frenkel effect is an electric field induced lowering of potential barrier for the thermal emission of a carrier from a level in the band-gap. We found that the high electrical field at the photodiode-transfer gate overlap was an important dark current mechanism in CMOS Image sensors in another work [18]. A 0.2 μm overlap is present between the pinned layer and the TX gate due to self-aligned process. A very strong electrical field of 3×10^5 V/cm is present in this region (when the reset voltage of the FD node is ~2 V) that gives rise to higher leakage current. This amounts to an emission enhancement factor of 18 in a 3-dimensional model [20]. Increasing the voltage on the TX gate moves the "pinch-off" point toward the photodiode region and results in an even higher electrical field. This phenomenon can be expected to be worse for future devices where the dimensions are made smaller and thus leading to higher electrical fields. Traps that are located in this high electric field region may exhibit a higher darker current than the traps located outside this local field. This could also lead to a higher RTS (random telegraph signal) noise in the sensor [5]. Clearly, further studies are necessary in this direction to establish the mechanism by which such electrical fields interact with traps introduced through irradiation and the effect of future aggressive technologies where dimensions are continuously being shrunk.

4. Conclusions

The GD technique is found to be a very simple and fast method to predict the radiation hardness of very complex and sensitive devices like CMOS image sensors. From the GD technique, it was found that threshold variations due to charge build-up as well as radiation induced leakage currents were negligible. γ-ray irradiation affects the spectral response of 4-T image sensors by altering the top layer material properties and changing the surface interface properties. For the dose rates considered in this work, both these phenomenon were found to vary monotonically with the dose as can be explained from the model that was developed. Further work needs to be done to characterize the top-layer material properties as a function of radiation dose for high quality imaging in future technologies. The results also indicate that p-well protected STI structures are inevitable for radiation-hard designs. A larger value of NTA results in higher immunity to radiation damage, but should be optimized to avoid loss of sensitivity and saturation levels of the sensor. With the shrinking of pixel size, the STI as well as the p-well fabrication processes would become the focus of attention for optimizing the process for high quality imaging

especially for applications related to harsh environments. Finally, with the shrinking geometries, higher electrical fields interact with radiation introduced traps thus contributing to a different leakage mechanism. From the above facts, it can be concluded that the deep submicron technology is a good candidate for fabricating CMOS image sensors for applications like medical imaging or outer space applications though some optimizations/studies in the direction presented in this work are necessary.

acknowledgements

This work is funded by the Dutch Technology Foundation (STW) DSC5869 and Philips/DALSA for test structures. The authors wish to thank Eric Bodegom, P.S.U; Adri Mierop, DALSA; Martijn Snoeij, TUDelft; Peter Swart, DIMES; and personnel of I.R.I, Delft, for their valuable insights and technical assistance during the project. Special thanks to Gregory Pandraud, DIMES-TUDelft for his valuable suggestions and guidance.

References

[1] Bogaerts J, Dierickx B, Meynants G, Uwaerts D. Total dose and displacement damage effects in a radiation-hardened CMOS APS. IEEE Trans Electr Dev 2003;50(1):84–90.
[2] Claeys C, Simon E. Radiation effects in advanced semiconductor materials and devices. Springer Ser Mater Sci 2002.
[3] Meng Xian-Ti, Kang Ai-Guo, Li Ji-Hong, Zhang Hai-Yun, Yu Shi jie, You Zheng. Effects of electron and gamma-ray irradiation on CMOS analog image sensors. Microelectron Reliab 2003;43(7):1151–5.
[4] Eid El-Sayed et al. Design and characterization of ionizing radiation-tolerant CMOS image APS image sensors 30 MRad (Si) total dose. IEEE Trans Nucl Sci 2001;48(6):1796–806.
[5] Hopkinson Gordon R. Radiation effects in a CMOS active pixel sensor. IEEE Trans Nucl Sci 2000;47(6):2480–4.
[6] Bogaerts J. Radiation-induced degradation effects in CMOS active pixel sensors and design of a radiation tolerant image sensor. PhD thesis, Katholieke University Leuven; April 2002. p. 5–15, 37–95.
[7] Moon CR, Jung J, Kwon DW, Yoo J, Lee DH, Kim K. Application of plasma-doping (PLAD) technique to reduce dark current of CMOS image sensors. IEEE Electr Dev Lett 2007;28(2):114–6.
[8] Riley LS, Hall S, Schitz J. Evaluation of surface generation velocity of sidewall oxide interfaces formed by dry etching for shallow trench isolation. Solid-State Electron 2000;44(11):2093–5.
[9] Bogaerts J, Dierickx B, Mertens R. Enhanced dark current generation in proton-irradiated CMOS active pixel sensors. IEEE Trans Nucl Sci 2002;49(3):1513–21.
[10] Rudenko T, Kilchytska V, Dessard V, Flandre D. A revised reverse gated-diode technique for determining generation parameters in thin-film silicon-on-insulator devices and its application at high temperatures. J Appl Phys 2005;97(9):093718.1–8.9.
[11] Roberts PCT, Beynon JDE. An experimental determination of the carrier lifetime near the $Si-SiO_2$ interface. Solid-State Electron 1973;16(2):221–7.
[12] Spiegel Jan Ver Der, Declerck Gilbert J. Theoretical and practical investigation of the thermal generation in gate controlled diodes. Solid-State Electron 1981;24(9):869–77.
[13] Grove AS, Fitzgerald DJ. Surface effects on p–n junctions: characteristics of surface space-charge regions under nonequilibrium conditions. Solid-State Electron 1966;9(September):783–806.
[14] Sinha A, Chatopadyaya SK. Photocurrent in a diffused p–n junction. Solid-State Electron 1976;19:345–6.
[15] Zhang X. Investigation of N^+–P diffused junction silicon solar cells. Solid-State Electron 1992;35(11):1661–5.
[16] Arshak K, Korostynska O. Gamma radiation-induced changes in the electrical and optical properties of tellurium dioxide thin films. IEEE Sens J 2003;3(6).
[17] Ohyama H et al. Defect assessment of irradiated STI diodes. Nucl Instrum Methods Phys Res Sect B 2002;186(1):424–8.
[18] Wang X, Rao PR, Theuwissen AJP. Fixed-pattern noise induced by transmission gate in pinned 4T CMOS image sensor pixels. In: Proceedings of ESSDERC; September 2006. p. 331-4.
[19] Kwon HI, Kang IM, Park BG, Lee JD, Park SS. The analysis of dark signals in the CMOS APS imagers from the characterization of test structures. IEEE Trans Electr Dev 2004;51(2):178–84.
[20] Srour JR, Hartmann RA. Enhanced displacement damage effectiveness in irradiated silicon devices. IEEE Trans Nucl Sci 1989;36(6):1825–30.
[21] Snoeys WJ, Palacios Gutierrez TA, Anelli G. A new NMOS layout structure for radiation tolerence. IEEE Trans Nucl Sci 2002;49(4):1829–33.
[22] Anelli G. Design and characterization of radiation tolerant integrated circuits in deep submicron CMOS technologies for the LHC experiments. PhD thesis, Institut National Polytechnique De Grenoble; December 2000. p. 39–44.